Article:
Parri, M.C., Qiu, Y. and Walther, T. (2015) New pathways for improved quantification of energy-dispersive X-ray spectra of semiconductors with multiple X-ray lines from thin foils investigated in transmission electron microscopy. Journal of Microscopy, 260 (3). pp. 427-441. ISSN: 1365-2818

https://doi.org/10.1111/jmi.12345

New pathways for improved quantification of energy-dispersive X-ray spectra of semiconductors with multiple X-ray lines from thin foils investigated in transmission electron microscopy,

New pathways for improved quantification of energy-dispersive X-ray spectra of semiconductors with multiple X-ray lines from thin foils investigated in transmission electron microscopy

M.C. Parri[1], Y. Qiu[1,2] and T. Walther[1,3]

[1] Department of Electronic & Electrical Engineering, University of Sheffield, Mappin Street, Sheffield S1 3JD, UK

[2] now at: IMEC, Kapeldreef 75, B-3001 Leuven, Belgium

[3] corresponding author: email: t.walther@sheffield.ac.uk,
telephone: +44 114 222 5891,
fax: +44 114 222 5143

Abstract: Theoretical approaches to quantify the chemical composition of bulk and thin layer specimens using energy-dispersive X-ray spectroscopy in a transmission electron microscope are compared to experiments investigating (In)GaAs and Si(Ge) semiconductors. Absorption correctors can be improved by varying the take-off angle to determine the depth of features within the foil or the samples thickness, or by definition of effective *k*-factors that can be obtained from plots of *k*-factors vs. foil thickness or, preferably, vs. the K/L intensity ratio for a suitable element. The latter procedure yields plots of self-consistent absorption corrections that can be used to determine the chemical composition, iteratively for SiGe using a set of calibration curves or directly from a single calibration curve for InGaAs, for single X-ray spectra without knowledge of sample thickness, density or mass absorption coefficients.

Keywords: energy-dispersive X-ray spectroscopy, analytical transmission electron microscopy, quantification, *k*-factors

Introduction

The basic principles of energy-dispersive X-ray spectroscopy (EDXS) in a transmission electron microscope (TEM) are well understood: by measuring the X-ray output of a material using a semiconductor detector it is often possible to determine the chemical composition to a good degree of accuracy. In very thin samples where X-ray absorption is negligible, quantification is hampered by two effects: the small numbers of X-rays produced in very thin foils mean that ***statistical*** errors will be high due to shot noise, and contributions from surfaces in the form of contamination or surface oxide layers (cf. Walther and Humphreys 1997) can be large relative to 'bulk' contributions from inside the thin foil specimens and cause ***systematic*** errors. Both effects could be reduced if thicker specimens were analysed, and in transmission electron microscopes operated at intermediate voltages (200-300kV) specimens of up to 1μm in thickness may be sufficiently electron transparent and can therefore be studied.

One of the primary difficulties then is correcting for absorption and fluorescence within the sample. The main parameters influencing absorption are chemical composition, density and thickness of the material that the X-ray travels through, i.e. mass-thickness of the sample, and take-off angle (Goldstein and Williams, 1981). Commercially available methods for determining the chemical composition require the sample thickness and density for approximate absorption correction, however calculating the thickness of the material travelled through could in principle be done without this directly from the X-ray spectrum

alone if several characteristic X-ray lines are present and the detector response function as well as the take-off angle were precisely known. This report seeks to expand on that idea and thus constitutes an alternative approach to the zeta-factor method of quantification where the specimen's chemistry and thickness can be iteratively determined if both mass absorption coefficients and the absolute electron dose employed are precisely known (Watanabe et al. 1996).

The absorption correction in the original Cliff-Lorimer ratio (Cliff & Lorimer, 1975) approach requires certain approximations: homogeneity along both the electron beam and X-ray paths and that the density and thickness of the sample are known a-priori.

The assumption of homogeneity along the electron beam and X-ray directions implies that minor local changes (such as due to stacking faults, impurities or the difference in chemistry between top and bottom parts of the foil) can be ignored. The result of this is that the quantity of X-rays produced and the number absorbed can be considered directly proportional to the volume and composition of the sample (given that the beam energy is sufficiently high so that the stopping power of the electrons does not vary significantly along the sample). A thicker material will produce more X-rays, and hence, knowledge of the sample's thickness is necessary to accurately estimate the number of X-rays initially produced. The density of a material has a correlation with the extent of absorption. Both of these factors have strong effects on correct quantification.

The effect of absorption is to decrease the X-ray intensity exponentially according to the following equation:

$$I = I_0 e^{-\frac{t^*}{\lambda}} \qquad (1)$$

where I and I_0 are the detected and generated X-ray intensities, respectively, t^* is the thickness of material the X-rays have travelled through and λ is the attenuation wavelength, which is a particular value depending on the energy of the X-ray and the material of the sample. The thickness t^* is generally given by

$$t^* = t/\sin\theta = t \operatorname{cosec}\theta \qquad (2),$$

where t is the vertical thickness of material between the origin of the X-ray and the sample surface and θ is the take-off angle. Division by sin θ (or multiplication by cosec θ) describes the increase in path length within the material X-rays have to travel through towards the detector placed under take-off angle θ, and smaller take-off angle means stronger absorption and fewer X-rays. It is worth noting that tilting the specimen by an angle α, as sketched in figure 2, increases the apparent specimen thickness by a factor of 1/cos*a,* creating correspondingly more X-rays and also changes the take-off angle, leading to decreased absorption if tilted towards but increased absorption if tilted away from the detector, and both angles need to considered for accurate quantification.

The number of X-rays detected from element j in a sample of thickness t is given by

$$I_\mathrm{j} = \frac{N_\mathrm{A}}{A_\mathrm{j}} \frac{i}{e} \rho t \, c_\mathrm{j} \, \sigma_\mathrm{j} \, \omega_\mathrm{j} \, f_\mathrm{j} \, a_\mathrm{j} \, e_\mathrm{j} \, \tau \qquad (3)$$

where N_A is Avogadro's constant, A_j the atomic weight of element j (in g/mol), i the probe current, e the electron charge, ρ the density, c_j the weight fraction, σ_j the ionisation cross-section, ω_j the fluorescence yield, f_j the line partitioning fraction (for K, L, M lines), a_j the absorption factor, e_j the detection efficiency of line j and τ the measurement time. Cliff and Lorimer (1975) developed the basic thin film quantification approach by defining a factor k_ij for two lines i,j as the ratio

$$k_\mathrm{ij} = \frac{\sigma_\mathrm{j} \, \omega_\mathrm{j} \, f_\mathrm{j} \, A_\mathrm{i} \, e_\mathrm{j}}{\sigma_\mathrm{i} \, \omega_\mathrm{i} \, f_\mathrm{i} \, A_\mathrm{j} \, e_\mathrm{i}} \qquad (4)$$

so that without absorption (i.e. for $a_\mathrm{j} = 1$) one simply obtains

$$\frac{I_\mathrm{j}}{I_\mathrm{i}} = \frac{c_\mathrm{j}}{c_\mathrm{i}} k_\mathrm{ij} \qquad (5).$$

The weight fraction is then given by

$$\frac{c_\mathrm{j}}{c_\mathrm{i}} = \frac{I_\mathrm{j}}{I_\mathrm{i}} k_\mathrm{ji} \qquad (6)$$

and the atomic fraction by

$$\frac{x_\mathrm{j}}{x_\mathrm{i}} = \frac{I_\mathrm{j} A_\mathrm{i}}{I_\mathrm{i} A_\mathrm{j}} k_\mathrm{ji} \qquad (7).$$

For a multinary system of n elements rather than a binary system, where $x_1+x_2+x_3+\ldots=1$, and with absorption, the Cliff-Lorimer method yields for atomic concentrations:

$$x_j = \frac{\frac{I_j k_j a_j}{A_j}}{\sum_n \frac{I_n k_n a_n}{A_n}} \qquad (8)$$

where n is an index running over all elements. The method requires that the k-factor be defined relative to a standard. In this report, that standard is $\mathrm{Si_K}$, which is the most common reference line. For shorthand we continue to write k_j if we refer to $k_\mathrm{j,SiK}$.

The k-factor and the absorption correction are intractably linked, as only their product, later-on called k^*, can be measured in an experiment. This is a significant problem, since the absorption and fluorescence correction will change depending on the thickness of the material while the k-factor would not. A method for calculating an effective k-factor including X-ray production, absorption, fluorescence and detection would therefore be of particular use.

In the following, we describe three approaches for obtaining additional quantitative information from X-ray spectra. Method 1 explores the consequences of specific inhomogeneity: when there is a discrete structure (e.g., a precipitate or a region of very high concentration of a certain element) embedded within the matrix of another composition then changing the take-off angle can yield information on the depth of the feature within the foil. This would be useful primarily for enhanced compositional analysis of embedded quantum structures, such as quantum wires (Cui, Robertson, Robinson, Andrei, Thompson, Botton, 2009) or nanoparticles (Tsen, Crozier, Liu, 2003; Zak, Laval, Dluzewski, Kret, Yam, Bouchier, Fossard, 2009). Method 2 attempts to calculate the thickness of a sample by comparing the X-ray output from several related lines, e.g. K/L intensity ratios, thereby permitting more quantitative analysis without needing to resort to other methods or rely on simulations. This has been suggested before (Morris, Ball, Statham, 1979; Horita, Ichitani, Sano, Nemoto, 1989) and would be most useful in samples with soft X-rays (Banchet, Michel, Jallot, Laurent-Maquin, Balossier, 2003; Ivetic, Nikolic, Parakevopulos, Pavlidou, Zorba, Nikolic, Ristic, 2008; West, Thomson, 2009; Laszcz, Czerwinski, Ratajcak, Szerling, Phillipp, van Aken, Katcki, 2010) or where, as in certain cases of medical samples (Kirk, Gates, Provance, Lee, 1997), an accurate knowledge of the thickness is critical for quantification of thicker samples where absorption cannot be neglected. Method 3 describes an aspect of how knowledge of the sample thickness or, preferably the K/L intensity ratio of a heavier element, can permit more accurate quantification, similar to a procedure described before (Horita, Ichitani, Sano, Nemoto, 1986; Horita, Sano, Nemoto, 1987 & 1991). As examples, semiconductors of technological importance, such as Si(Ge) and (In)GaAs have been chosen.

Experimental

All the experimental data presented here was gathered with a JEOL 2010F field-emission transmission electron microscope (TEM) operated at 197kV, equipped with an URP pole-piece with 2mm pole-piece gap, and a Si:Li detector with 25° nominal take-off-angle, ultrathin polymer window, Oxford Instruments ISIS 300 software, specimen tilt range approximately -10° to +25°. Specimens investigated included:

i. GaAs wedge specimens, cleaved and viewed along <100> zone axis,
ii. InGaAs plan-view specimens, studied near <001> zone axis,
iii. InGaAs/GaAs cross-sections studied near <110> zone axis, all polished and argon ion milled for perforation,
iv. SiGe/Si: as under iii. above

For comparing experimental and simulated data on absolute scales, as in Figures 1, 5, 8 and 9, the efficiency of our X-ray detector has been calculated with the DTSA-II code (Ritchie, 2009) and the resulting estimated detector efficiencies are listed in Table 1 for the relevant X-ray lines considered.

Monte Carlo simulations

Four Monte Carlo programs were used to provide simulated data for comparison with experimental results. These four were NISTMonte (Ritchie, 2005), CASINO (Hovington, Drouin & Gauvin, 1997), Hurricane (Rickerby & Thiot, 1994) and EDAX Electron Flight Simulator (EEFS) (Smallworld, 2012). EEFS does not apply relativistic corrections to the scattering and ionisation cross-sections, and as such would likely give incorrect results for the high beam energies used here, however, for ratios, a lack of relativistic corrections should

cancel out. EEFS only allows a maximum thickness of 3µm to be simulated, hence its graph is truncated. All simulations were carried out for 1 million electron trajectories at 200keV and assumed a detector efficiency of unity, while Table 1 suggests a ratio of e_{AsK}/e_{AsL}=1.16 in the experiment.

Figure 1 compares the simulated and experimental results of the As_K/As_L line intensity ratio from a homogenous GaAs 90º wedge sample tilted very slightly off a [100] zone axis orientation, on a double-log plot so an upwards shift of 16% of the experimental data will be irrelevant. Experimental thicknesses were measured as twice the distance from the edge, which is difficult to assess for very large thicknesses where the specimen appears pitch-black in bright-field TEM mode and the magnification has to be reduced far enough so the edge can actually be seen (while LOW MAG mode with the objective lens switched off has to be avoided for EDXS as high energy electrons could directly hit the detector). All curves have a similar form, with an inflection point around a thickness of ~2µm, indicating the absorption is modelled with similar attenuation lengths in all of them. It is clear that the results from NISTMonte and CASINO match the experimental much more closely than HURRICANE or EEFS that are lower by factors between ~4x and ~30x (Walther, 2010a), which must be due to incorrect ionisation cross-sections and/or fluorescence yields in the latter codes (only their product enters in equation 3). Despite some outliers in experimental measurements (presumably due to the difficulty in assessing very large thicknesses in experiments), we conclude that if one wants to model X-ray absorption, one can either use tabulated values for mass attenuation coefficients, e.g. from NIST (Hubbell and Seltzer 1996), or Monte Carlo codes like NISTMonte or CASINO. We have chosen the latter to get a direct output of intensities vs. specimen thickness for alloys not listed in these tables without having to assume constant ionisation cross-sections along the electron beam path. The main point of

Figure 1 is thus to show that ionisation cross-sections (determining the height of the curves), and thus also corresponding thin film *k*-factors, are less well predicted than X-ray absorption lengths (that determine the form of the curves).

Method 1: calculation of depths of features embedded within specimens from range of specimen tilts

If there is a local structure or high concentration of a material embedded within a matrix of another material, the assumption of the Cliff-Lorimer approach that the X-rays originate equally from all points within the beam interaction volume is not valid.

It has been shown (Walther, 2008) that the intensity of detected X-rays, I, can be expressed analytically as a function of generated intensity, I_o, by:

$$I = I_o \exp^{-\frac{D}{\lambda}} \qquad (9)$$

where $D = d$ cosec θ is the length of material the X-rays have effectively travelled through to reach the detector, as sketched in Figure 2a, and λ is the attenuation wavelength, a constant for a given X-ray energy in a specific material. For an infinitely thin layer imaged at depth d the electron beam transverses perpendicularly, this can be algebraically reduced to

$$d = \frac{\lambda \ln\left(\frac{I_1}{I_2}\right)}{\text{cosec } \theta_2 - \text{ cosec } \theta_1} \qquad (10a)$$

Assuming that the feature has a well defined depth within the foil and that its self-absorption can be neglected, this equation would permit the calculation of the depth of the X-ray source, in turn allowing a more accurate absorption correction and ergo better quantification.

Unfortunately, most microscopes do not allow for the detector to be moved to vary the take-off angle. This can be substituted by tilting the specimen when a change in take-off angle is required, as sketched in Figure 2b. However, doing so noticeably increases the effective specimen thickness in projection and thus the interaction volume, by a factor of $1/\cos\alpha$. The detected intensity must be multiplied by the cosine of the specimen tilt angle to convert the experimental intensity to what would be expected from a flat horizontal sample and a modelled tilted detector. In the following, this correction, which for tilts from α=−10° to +25° range amounts to relative corrections of up to $1/\cos 25° - 1 = 10.3\%$, has been applied throughout to all experiments and simulations with tilted specimens, i.e. equation (10a) for detector tilt effectively turns into equation (10b) for specimen tilt:

$$d = \frac{\lambda \ln\left(\frac{I_1 \cos a_1}{I_2 \cos a_2}\right)}{\operatorname{cosec}\theta_2 - \operatorname{cosec}\theta_1} \qquad (10b)$$

Note that the cosine factors are due to changes in projected thickness (when tilting the specimen) while the cosec factors are due to the change in take-off angle. The angular correction to the numerator in equation (10b) depends strongly on the intensity ratio I_1/I_2 and is maximal if this intensity ratio approaches unity, as the logarithm function then has the largest gradient (note $I_1 > I_2$ for $|\alpha_1| > |\alpha_2|$ guarantees the logarithm is only ever evaluated for values >1). A major experimental issue was that, despite experiments close to the eucentric height, any large specimen tilts led to some lateral displacements which we tried to compensate by careful lateral movement of the specimen holder by the piezo stage to retain the weak contrast features visible in plan-view geometry in order to ensure that the same position was investigated all the time.

Figure 3 illustrates the simulated curve expected from a thin layer with changing take-off angle for a 1nm thick InAs layer embedded 50nm deep within a GaAs sample 120nm thick. The form of the exponential curve of 'detected intensity' describes the X-ray intensity including absorption and is characteristic for the tilted sample geometry, regardless of material. The 'generated intensity' curve is much flatter (note the enlarged scale of the right vertical axis) and demonstrates that the geometrical correction for tilt (multiplication by cos α) is not entirely effective, as a perfect correction would result in no change in X-ray generation with changing tilt at all. The change observed is due to the electrons in the beam losing energy as they travel through more material and therefore experiencing an increased stopping power, which in turn increases X-ray generation. The change in the 'generated intensity' is very small (<1%) in comparison to the 'detected intensity'.

Table 2 contains the results from applying equation (10b) to the simulated data of Figure 3. It is clear that the numerical evaluation is working well for low tilts but becomes increasingly incorrect with greater take-off angles. The beam straggling effect means that any fit calculated from two relatively high tilts should be ignored: precisely what tilt range can be used will be dependent on the X-ray in question and the thickness and composition of the capping layer and the accuracy required. For the tilt range $-10° < \alpha < 20°$ the average value and the standard deviation from the output of these simulations is 51.7±1.5nm, which is 2.3±3.0% higher than the input value of 50.5nm (for all values the result would be 52.5±3.1nm). It is worth noting that the input data has an expected standard deviation of less than 0.02% in these simulations, based on 3×10^7 X-ray events simulated, implying that even small systematic changes in the measured intensity would result in much larger errors in the evaluation. Assuming equal errors from Poisson counting statistics and background extrapolation, this would mean line intensities in the order of 10^8 would be necessary for

comparable accuracy in any experiment, which would be impractical for most experiments. However, such high count rates would only be necessary in a system that has such a small quantity of the material of interest (here, a 1nm InAs embedded in 50nm GaAs means an effective indium concentration of ~1at%): a greater amount of indium would see a lower requirement for counts.

This method was applied to an 8nm thick $In_{0.24}Ga_{0.76}As$ layer embedded 95nm deep within GaAs. Layer thickness, position and composition were confirmed by analysis of a cross-sectional sample, as shown in Figure 4.

Figure 5 shows the In_L intensity detected from this sample at different experimental tilts from -10º to +18º. For large tilts away from the detector ($\alpha \leq -11º$) the holder shielded X-rays emission completely, which is not taken into account in the simulation. This shadowing effect explains the pronounced fall-off in counts for such tilts. It is clear that while the statistics are poor, as only ~1% of the sample volume is occupied by In atoms contributing to the signal, the overall trend of the curve matches the simulations.

Looking at Figure 6, which tries to recover the layer depth numerically, it is however clear that no legible answer is available. This appears to be a consequence of the data's poor statistics, which is itself a result of attempting to acquire a large number of spectra (i.e. intensities for the maximum number of tilts) for a weak signal.

However, another method can also be applied to the same data: by simulating the 8nm $In_{0.24}Ga_{0.76}As$ with different GaAs overlayer thicknesses it would be theoretically possible to discover the closest match between the experimental and simulated curves and thereby find

what depth the simulations imply to be the correct value. This closest match can be found by plotting the sum of squares against simulated overlayer thickness, where the minimum would be the most likely, and hopefully correct, answer. Since the experimental and simulated data are on different absolute scales, it is necessary to normalise the simulated data to the same scale as the experimental. As no experimental data point would be ideal for normalising with respect to, the normalisation has been carried out with respect to all experimental data points individually. Not every curve possesses a minimum: these would be the result of the experimental data point being so far from the expected curve that the simulations either continually move away or converge above some unphysical overlayer thickness (in this case, >200nm). Further, some smoothing was attempted by averaging over two ('pairs') or three ('triplets') data points.

Attempting this method using the In_L intensities alone does not give reasonable answers: most curves give a result larger than 200nm. However, applying the same procedure to the measured In_L/As_K ratio does give meaningful results, as seen in Figure 7. The values calculated here are not only physically reasonable but agree with the true depth value, albeit with large error bars. The difference in behaviour between the In_L and In_L/As_K results could be due to the large scatter from statistics being counteracted by the normalisation by As_K.

In summary, a fairly typical sample was examined using equation (10b) and it was found that inferior statistics could produce so much scatter as to invalidate the approach. However, comparing experimental intensity *ratios* to simulated results does seem to give reasonable answers. While such a comparison to simulations is time consuming to carry out it does show some promise by extracting meaningful results from experiments with even rather poor statistics. If the depth of features, such as quantum wells, quantum dots or precipitates, within

a specimen foil can be determined from comparative measurements at different tilts, then absorption corrections for X-rays can be improved and a higher reliability of any compositional estimate may be obtained. In the above example, the depth of the flat InAs layer beneath the surface of a GaAs specimen could be predicted with about ±10% relative accuracy, corresponding to ~10nm, as given by the mean peak position error of fitting a distribution to the histogram in Figure 7, however, the width of the distribution as given by the random mean square error is much larger (~50nm), and more complicated shapes of buried features could have a profound effect on the variation of an X-ray intensity ratio with specimen tilt. In conclusion, we propose to use experimental X-ray intensity ratios and perform a multiple least-squares fit to all possible combinations of tilt angles to determine the most likely depth of a feature in the foil from equation (10b). This can then be used to improve standard X-ray absorption corrections, although the scatter of the resulting numerical depth values obtained may remain rather large due to limited signal-to-noise ratios in typical X-ray spectra.

Method 2: determination of sample thickness from K/L intensity ratios

The degree of absorption for a particular X-ray line is dependent on three factors: the density and composition of the material travelled through, the amount of material to travel through, and the energy of the X-ray. By analysing different X-ray lines (i.e. those with different energies) for the same element from the sample in the same geometry, it is possible to deduce the extent of absorption. By then studying areas of different thicknesses of the sample while still analysing the same two X-ray lines, it should be possible to calculate the effect that thickness has on absorption. If the ratio of these two X-ray lines are plotted for many different thicknesses, it would be possible to examine samples of different chemical

composition and density who exhibit the same set of X-ray lines (amongst possibly many others) more quantitatively by deriving their sample thickness affecting absorption by interpolating between points on this calibration curve.

Based on this idea, different ways of parameterisation of absorption have been tested over the decades: Morris, Ball and Statham (1980) plotted Cu/Al compositional ratios vs. mass absorption coefficients where the latter had to be iteratively fitted to Cu K/L line ratios. Horita, Sano and Nemoto (1986) plotted an effective *k*-factor vs. absolute specimen thickness measured in nanometres, which they showed later is rather difficult to experimentally measure reliably (Horita *et al.*, 1989). Horita, Sano and Nemoto (1987) and van Cappellen (1990) also plotted atomic ratios vs. the measured total intensity of a specific (hard) X-ray line to perform an absorption correction, however, absolute X-ray counts will depend on the total beam intensity and thus will only be comparable for a series of measurements in one specific microscope under exactly the same conditions. All these parameterisations need series of measurements to extrapolate the effect of absorption down to zero thickness to get the Cliff-Lorimer *k*-factor appropriate for thin films.

In the following we show that simulations suggest almost linear changes of K/L intensity ratios with specimen thickness over ranges typical of foils examined in transmission geometry, however, numerical results from different simulation programs differ by so much that the endpoints for reliable fits must be obtained from experimental measurements. In particular, the assumption of simple analytical models that the average X-ray emission event occurs in the middle of the foil neglects not only any fluorescence but also the strong non-linearity of the absorption of softer X-rays, which means that the intensity from the middle of the foil is actually higher than the simple average from top and bottom sides of the foil.

Therefore, substituting tabulated X-ray absorption lengths into an exponential absorption curve assuming half the foil thickness will be inappropriate, and we again used Monte Carlo simulations to predict X-ray intensities. For small thicknesses, an alternative would have been to perform a simple line integral of an absorption-modified X-ray intensity assuming uniform ionisation along the electron path, however, neglecting beam straggling and stopping power variations is only permissible up to ~100nm for 200kV electrons, while our simulations cover a range up to 2μm thickness and experimental data are for lamellae up to ~1μm thick..

Figure 8 compares results for GaAs using NISTMonte and CASINO simulations, with same detector sensitivities, to experiments. Up to 2μm thickness the simulated plots are nearly linear. As demonstrated in Figure 1, this pattern does not hold beyond a certain thickness but should be valid for typical specimen thicknesses in transmission electron microscopy. The difference between the two programs is consistent with that of Figure 1. The experimental data was gathered from four areas of a lamella that had been milled by a focused ion beam (FIB) to the specified thicknesses. It seems clear that the experimental data deviate significantly from the simulated results, in that the CASINO Ga K/L ratio agrees with the experimental data better than NISTMonte, while the reverse is true for the As K/L ratio. This is troublesome, as it implies that neither program can be relied upon to give results that are directly comparable to experiment, even if detector sensitivities are taking into account. More experimental data points at different thicknesses would aid the choice of the best fitting simulated curve by simply improving the reliability of the linear least-squares fit.

Figure 9 shows similar simulations for a SiGe sample (Ge K/L only, as Si does not have an easily quantifiable L-line).

Table 4 compares the linear least-squares regression of the data in Figure 9. It can be seen that CASINO has higher scatter and lower R^2, in addition to beginning higher and increasing slightly faster. Recently determined experimental results (Qiu et al., 2013) indicate that the correct value for the intercept would be 1.30±0.05, which agrees with CASINO but disagrees with NISTMonte.

The major conclusion is that the K/L ratio appears to remain linear over useful ranges of TEM specimen thicknesses. The consequence of this is that very few data points would be needed to construct such a plot for any material, as it is simply a matter of linearly extrapolating from the available points. In effect, the number of points needed is more strongly dependent on their error bars than any other factor, and in principle a K/L intensity ratio for a very thin sample ($t \rightarrow 0$nm) and another values for a thick sample area of well-known thickness (e.g. 1μm) would be sufficient. The experimental problem will be to obtain X-ray measurements for a precisely known large thickness, say ~1μm with an error of less than 20nm, which could serve as upper calibration point. Then, in related samples of similar density and/or composition, a simple K/L intensity ratio extraction would allow a quick thickness estimate and hence a more reliable absorption correction using standard software.

Method 3: Improved accuracy of chemical composition measurement by sets of thickness-dependent *k*-factors

The '*k*-factor' of the Cliff-Lorimer method is defined relative to another X-ray line. Generally, this line is Si_K though Fe_K is sometimes used. As such, in the specific case of $Si_{1-x}Ge_x$, $k_{SiK} = 1$ by definition, $a_{SiK} = 1$ by defining the absorption relative to that of Si_K for simplicity and $x = x_{Ge} = 1 - x_{Si}$, which permits reducing the calculation of the effective *k*-factor, k^*, for the germanium lines to

$$k^*_{Ge_{K,L}} \equiv k_{Ge_{K,L}} a_{Ge_{K,L}} = \frac{x}{(1-x)} \frac{I_{Si} A_{Ge}}{I_{Ge} A_{Si}} \quad (11)$$

where, again, *I* describes the measured intensities (now in thicker samples) and *A* the atomic weights. This *k** factor is the product of the classical thin film *k*-factor from equation (4) and the absorption correction factor *a* from equation (3).

We can only separate the *k*-factor and absorption terms for t=0 where absorption is negligible (a≈1), and in practice *k*-factors have often been measured for samples assumed to be sufficiently thin to assume a = 1, usually without this having been proven. This can be better achieved by calculating values of k^* for a number of data points with decreasing sample thickness, and extrapolating to zero thickness, as the k^* values at zero thickness would have an absorption of unity (Horita, McCartney and Weiss, 1992; Walther, 2010b). k^* would then be a thickness dependent *k*-factor which would permit more accurate quantification of homogenous or near homogenous samples of known thickness. If a reliable thickness value is not available and the estimate is wrong, then quantification results from K- and L-lines from the same element (here Ge_K and Ge_L) would differ. This may be improved, rather than by averaging, by choosing a thickness value consistent with the experimentally measured K/L ratio (see method 2 and Morris, Ball, Statham, 1980; Horita, Ichitani, Sano, Nemoto, 1989).

Figure 10 shows simulated and experimental results for $Si_{0.54}Ge_{0.46}$ (Qiu et al., 2013). It is clear that while the general form of the trend is consistent between simulation programs and experimental results, the curvature and termination points of the curves differ considerably. Of the two programs, CASINO appears to be closer to experiment in this case. Extrapolating using a second order polynomial yields k^* at t=0 for Ge_K of $1.491\pm^{0.093}_{0.089}$ and Ge_L of $2.004\pm^{0.075}_{0.072}$, whereas Oxford Instruments' ISIS software gives values of 1.609 and 1.654, respectively.

Figure 11 shows plots of k*-factors simulated by CASINO for both Ge lines (L at the top, K at the bottom) for germanium concentrations of x=0.1, 0.3, 0.5, 0.7 and 0.9. While the latter two sets for x=0.7 and 0.9 almost overlap, sets for low Ge concentrations yield different calibration curves for k* vs Ge K/L intensity ratio. As all curves are monotonic, do not cross and are sorted so the ones for lowest Ge concentrations yield the largest k*-factors, it is possible to iteratively determine x, and the result is independent of the starting curve used. If for example, a 1050nm thick (!) $Si_{0.8}Ge_{0.2}$ specimen yields a Ge K/L ratio of 1.644 and one looks this K/L value up in the calibration curves for x=0.1 [0.3] then the estimated k^*_{GeL} factor would be 2.361 [1.699], which from the measured intensities would predict x=0.231 [0.178]. So, curves with a too low [high] reference value would predict too high [too low] values for k* and thus also x. Hence, the problem is solely to find iteratively the correct calibration curve, which is given by the one for a value x_{cal} that best matches the value x_{out} if the corresponding k*-factor from this curve is used. This ensures self-consistency for quantification using either Ge L or K lines. The precision is merely a matter how densely sampled the calibration curves are. In our case, with an increment of only Δx=0.2, we by interpolation get x=0.205±0.027 from the Ge L quantification curves for x=0.1 and 0.3 (and a very similar value for Ge K quantification). For x<0.1 one would need a few more curves for lower reference compositions (x=0.02, 0.04 and 0.07 may suffice) as these are more widely spaced for same Δx increments than for higher x values. For x>0.7 the calibration curves are so similar that no iteration will be needed as it would not matter which one was used.

In the more general situation where silicon is not present, the k-factor of the second material will not be equal to unity. However, a k-factor calculated relative to another element will implicitly also be relative to whichever line that other k-factor was calculated with respect to, as $k_{AB} = k_{AC} * k_{CB}$ by definition. This is true for thin-film k-factors and k*-factors plotted vs

K/L line ratios if the densities of the compounds the X-ray lines are measured from do not change too much, but not if the latter were plotted as function of absolute thicknesses as in Figure 12.

At the moment, there are no corrected *k*-factors for the $Ga_{K,L}$ or $As_{K,L}$ lines that would allow them to be expressed relative to Si_K. As such, the k^* calculated in Figures 12 and 13 are with respect to the As_K line, as this has the highest energy and therefore is the least absorbed.

Simulated results indicate that an appropriate fit against K/L ratio (cf. Figure 11 for SiGe) would be at least second order polynomial. The results of a similar fit to Figure 12 are shown for GaAs in the third column of Table 5, with the 10nm data point (which simulations indicate is an outlier) either included or omitted, respectively: this would give values for *k*-factors extrapolated to zero thickness. Values for these standard *k*-factors, taken from Oxford Instruments ISIS software, are shown for comparison. Obviously, these are defined with respect to Si_K so the values shown here were calculated as $k_{AB} = k_{A,SiK} / k_{B,SiK}$. Unfortunately, while the Ga_K/As_K data are plausible and have sufficiently small relative errors to be useful, the remaining lines either scatter too much or, as for As_L/As_K without the 10nm data point, are unphysical. Figure 12 demonstrates that direct measurements of *k*-factors from thin samples can show systematic artefacts (due to surface damage during preparation, oxidation or irradiation damage), compared to an extrapolation from a series of measurements with improved statistics at higher thicknesses.

Attempting this analysis with respect to As_K/As_L or Ga_K/Ga_L intensity ratios plotted vs. As K/L line intensity ratio instead of absolute thickness gives the improved results shown in Table 6. Note that the corrected *k*-factors for As_L/As_K cannot meaningfully be plotted against

As_K/As_L. In these cases, it was not necessary to exclude any data points, as those which were previously outliers now lie much closer to the expected curve, as seen in Figure 13. Here, the R^2 goodness of fit values are uniformly higher and all values are physically reasonable, indicating that the resulting values are superior to those seen in Table 5. In theory, it would be expected that the k*-factor value for an X-ray line plotted vs. As_K/As_L or Ga_K/Ga_L would be identical if extrapolated to t=0: differences may be attributed to numerous factors such as incorrect detector efficiencies or K/L intensity ratios extrapolated to $t = 0$. For the Ga_K line, k-factors extrapolated from plots vs As K/L and Ga K/L agree to within 3%.

Experimentally, there are two different ways to determine k*: either by determining the absolute sample thickness or indirectly via the K/L ratio. While absolute specimen thicknesses are experimentally difficult to measure to high accuracy and would necessitate independent data from other methods (such as electron energy-loss spectroscopy or convergent beam diffraction if the specimen geometry were not known a-priori), choosing K/L intensity ratios instead as the horizontal axis instead means we rely only on data from X-ray spectra and so obtain an inherent self-calibration. The advantage of the K/L ratio method thus is that the result is always self-consistent for the area being examined (since the same data set is being used).

In analogy to equation (11), k*-factors for the In L-line in an $In_xGa_{1-x}As$ alloy can be defined with respect to a Ga line as

$$k^*_{In_{L,Ga}} = \frac{I_{Ga}A_{In}}{I_{In}A_{Ga}} \frac{x}{1-x} \qquad (12)$$

or, with respect to an As line, as

$$k^*_{In_{L,As}} = \frac{I_{As}A_{In}}{I_{In}A_{As}} x \qquad (13).$$

Figure 14 finally plots CASINO simulations of $k^*_{InL,As}$ for both As lines (top: As_L for reference, bottom: As_K for reference). Note that if we plot k* vs. As K/L intensity ratio, then

the values for different alloy concentrations move along EXACTLY THE SAME LINE as the thickness is changed but all fall onto one universal curve for all values of *x* considered. If the In content for $In_xGa_{1-x}As$ is changed, or if the thickness is changed, then absorption affects also the As K/L ratio value and one would simply move along the SAME curve to a DIFFERENT POINT. If we plotted $k^*_{InL,Ga}$ for both Ga lines as function of Ga K/L ratio instead, then the situation would be rather similar to the situation for $Si_{1-x}Ge_x$ considered before and we would need a set of calibration curves for different concentrations, which could be solved iteratively.

The general validity of the above proposed approach of using a K/L ratio measurement from an experimental X-ray spectrum for a self-consistent absorption correction has recently been demonstrated for various In and Ga containing compound semiconductors (Walther and Wang 2015), with an emphasis on InGaN where only the Ga K/L ratio can serve as thickness reference. We could also show that this method is rather insensitive to variations in detector sensitivities and so should be rather widely applicable.

Conclusion

Three methods describing more effective quantification of X-ray spectra in analytical TEM have been presented. To summarise: plotting K/L ratio against sample thickness gives an approximately linear curve for sample thicknesses ≤1μm, it may be possible to exploit the geometric change induced by changing the take-off angle to determine the depth of a buried thin layer (if it lies in a range where the absorption of the corresponding X-ray changes noticeably), and refining the process for calculating effective *k*-factors based on an indirect absorption correction resulting from consistent K/L quantification appears to be possible, as shown explicitly for the Ga K-line in GaAs. Plotting effective *k*-factors vs. K/L intensity

ratios, ideally for an element whose concentration is fixed (as for As K/L in a pure arsenide compound), is preferable to plots as function of absolute specimen thickness.

Acknowledgement

The authors would like to thank two very knowledgeable reviewers whose critical remarks have considerably strengthened the manuscript.

References

Banchet V., Michel J., Jallot E., Laurent-Maquin D. and Balossier G. (2003) Light elements quantitative x-ray microanalysis of thin samples in STEM. Absorption correction using EELS data. *J. Phys. D: Appl. Phys.* **36**, 1599-1604.

Cliff G. and Lorimer G.W. (1975) Quantitative analysis of thin specimens. *J. Microscopy* **103**, 203-207.

Cui K., Robertson M.D., Robinson B.J., Andrei C.M., Thompson D.A. and Botton G.A. (2009) Quantitative compositional analysis and strain study of InAs quantum wires with InGaAlAs barrier layers. *J. Appl. Phys.* **105**, 094313.

Goldstein J.I. and Williams D.B. (1981) X-ray microanalysis of thin specimens, in: Proc. Quantitative Microanalysis with High Spatial Resolution, Manchester (eds. G.W. Lorimer, M.H. Jacobs and P. Doig), pp. 5-14. The Metals Society, London.

Horita Z., Sano T. and Nemoto M. (1986) An extrapolation method for the determination of Cliff-Lorimer k_{AB} factors at zero foil thickness. *J. Microscopy-Oxford* **143**, 215 -231.

Horita Z., Ichitani K., Sano T. and Nemoto M. (1989) Applicability of the differential X-ray absorption method to the determination of foil thickness and local composition in the analytical electron microscope. *Philos. Magazine A* **59**, 939-952.

Horita Z., Sano T. and Nemoto M. (1987) Simplification of X-ray absorption correction in thin-sample quantitative microanalysis. *Ultramicroscopy* **21**, 271-276.

Horita Z., Sano T. and Nemoto M. (1991) A new form of the extrapolation method for absorption correction in quantitative X-ray microanalysis with the analytical electron microscope. *Ultramicroscopy* **35**, 27-36.

Horita Z, McCartney, MR and Weiss JK (1992) Computer-assited extrapolation method for absorption correction in quantitative X-ray microanalysis. *Ultramicroscopy* **45**, 263-265.

Hovington P., Drouin D. and Gauvin R. (1997) CASINO: A new Monte Carlo code in C language for electron beam interaction.1. Description of the program. *Scanning* **19**, 1-14.

Hubell J.H. and Seltzer S.M. (1996) Tables of X-ray Mass Attenuation Coefficients and Mass Energy-Absorption Coefficients from 1keV to 20MeV for Elements Z=1 to 92 and 48 Additional Substances of Dosimetric Interest, http://www.nist.gov/pml/data/xraycoef/

Kirk R.G., Gates M.E., Provance A.J. and Lee P. (1997) Quantitative X-ray images calculated on the basis of mass and volume. *Microsc. Microanal.* **3**, 512-519.

Liew S.L., Walther T., Irsen S., Hopkinson M., Skolnick M.S. and Cullis A.G. (2007) Investigating the capping of InAs quantum dots by InGaAs. *Springer Proc. in Physics*, **120**, 259-262.

Morris P.L., Ball M.D. and Statham P.J. (1980) The correction of thin foil microanalysis data for X-ray absorption effects. Proc. EMAG 1979 conference, *Inst. Phys. Conf. Ser. No.* **52**, 413-416.

Qiu Y., Nguyen V.H., Dobbie A., Myronov M. and Walther T. (2013) Calibration of thickness-dependent *k*-factors for germanium X-ray lines to improve energy-dispersive X-ray spectroscopy of SiGe layers in analytical transmission electron microscopy. Proc. 18th Microsc. Semicond. Mater., Oxford. *J. Phys. Conf. Ser.* **471**, 012031.

Rickerby D.G. and Thiot J.F. (1994) X-ray microanalysis of thin-film layered specimens containing light elements. *Mikrochimica Acta* **114**, 421-429.

Ritchie N.W.M. (2005) A new Monte Carlo application for complex sample geometries. *Surf. Interface Anal.* **37**, 1006-1011.

Ritchie N.W.M. (2009) Spectrum simulation in DTSA-II. *Microsc. Microanal.* **125**, 454-468.

SmallWorld. http://www.small-world.net/efs.htm [Online] 2012. [Cited: 27 November 2012.]

Tsen S.-C.Y., Crozier P.A. and Liu J. (2003) Lattice measurement and alloy compositions in metal and bimetallic nanoparticles. *Ultramicroscopy* **98**, 63-72.

Van Cappellen, E. (1990) The parameterless correction method in X-ray microanalysis. *Microsc. Microanal. Microstruct*. **1**, 1-22.

Walther T. and Humphreys C.J. (1997) Quantification of the composition of silicon germanium/ silicon structures by high-angle annular dark-field imaging. Proc. EMAG 1997, Cambridge. *Inst. Phys. Conf. Ser.* **153**, 303-306.

Walther T. (2008) A simple method to improve the quantification accuracy of energy-dispersive X-ray microanalysis. Proc. EMAG 2007 conference, Glasgow (eds. R.T. Baker, G. Möbus and P.D. Brown) *J. Phys.: Conf. Ser.* **126**, 012090.

Walther T. (2010a) Comparison of experimental and theoretical X-ray intensities from (In)GaAs specimens investigated by energy-dispersive X-ray spectroscopy in a transmission electron microscope. Proc. 16th MSM, Oxford (eds. T. Walther, P.D. Nellist, J.L. Hutchison and A.G. Cullis) *J. Phys.: Conf. Ser.* **209**, 012029.

Walther T. (2010b) An improved approach to quantitative X-ray microanalysis in (S)TEM: thickness dependent *k*-factors. Proc. EMAG 2009 conference, Sheffield (ed. R.T. Baker) *J. Phys.: Conf. Ser.* **241**, 012016.

Walther T. and Wang X. (2015) Self-consistent method for quantifying indium content from X-ray spectra of thick compound semiconductor specimens in a transmission electron microscope. *J. Microsc.,* in print, doi: 10.1111/jmi.12291

Watanabe M., Horita Z. and Nemoto M. (1996) Absorption correction and thickness determination using the zeta factor in quantitative X-ray microanalysis. *Ultramicroscopy* **65**, 187-198

Williams D.B and Carter C.B (1996) Transmission Electron Microscopy, Plenum Press, New York.

Zak M., Laval J.-Y., Dluzewski P.A., Kret S., Yam V., Bouchier D. and Fossard F. (2009) Influence of the Si cap layer on the SiGe islands morphology. *Micron* **40**, 122-125.

Figures

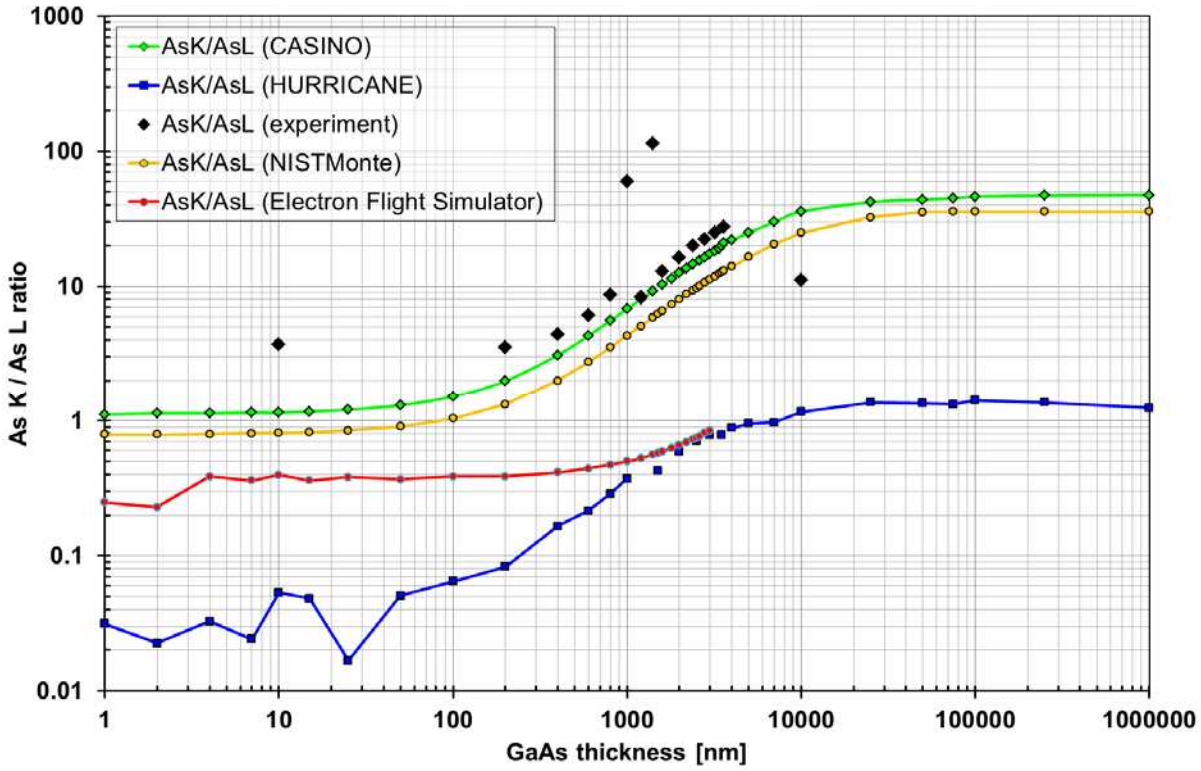

Figure 1: Comparison of X-ray intensity ratios from simulation programs to experimental data for pure GaAs.

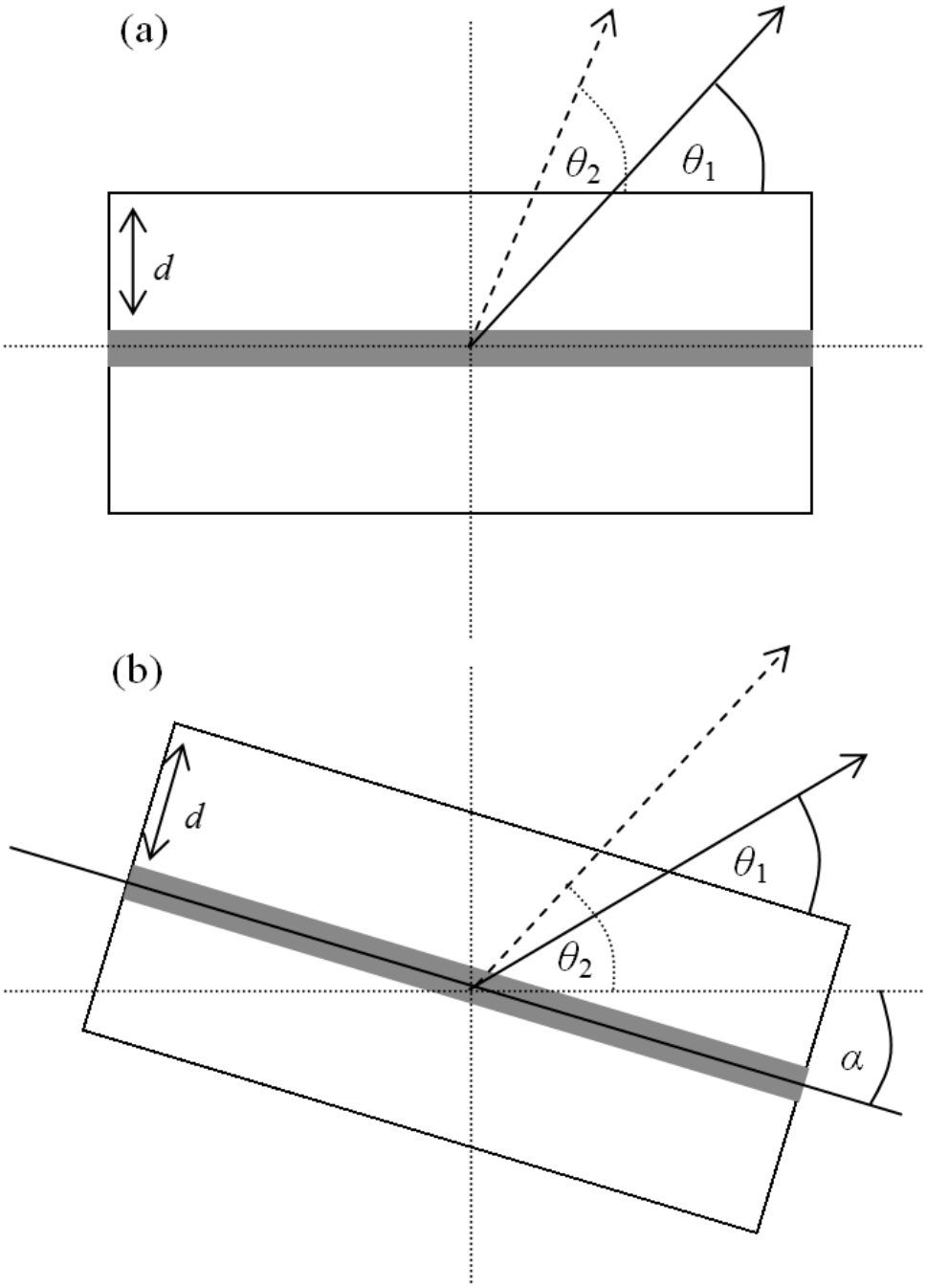

Figure 2: Geometric diagram of system for different take-off angles: (a) principle and (b) experimental implementation via specimen tilt so that $\theta_2 = \theta_1 + \alpha$.

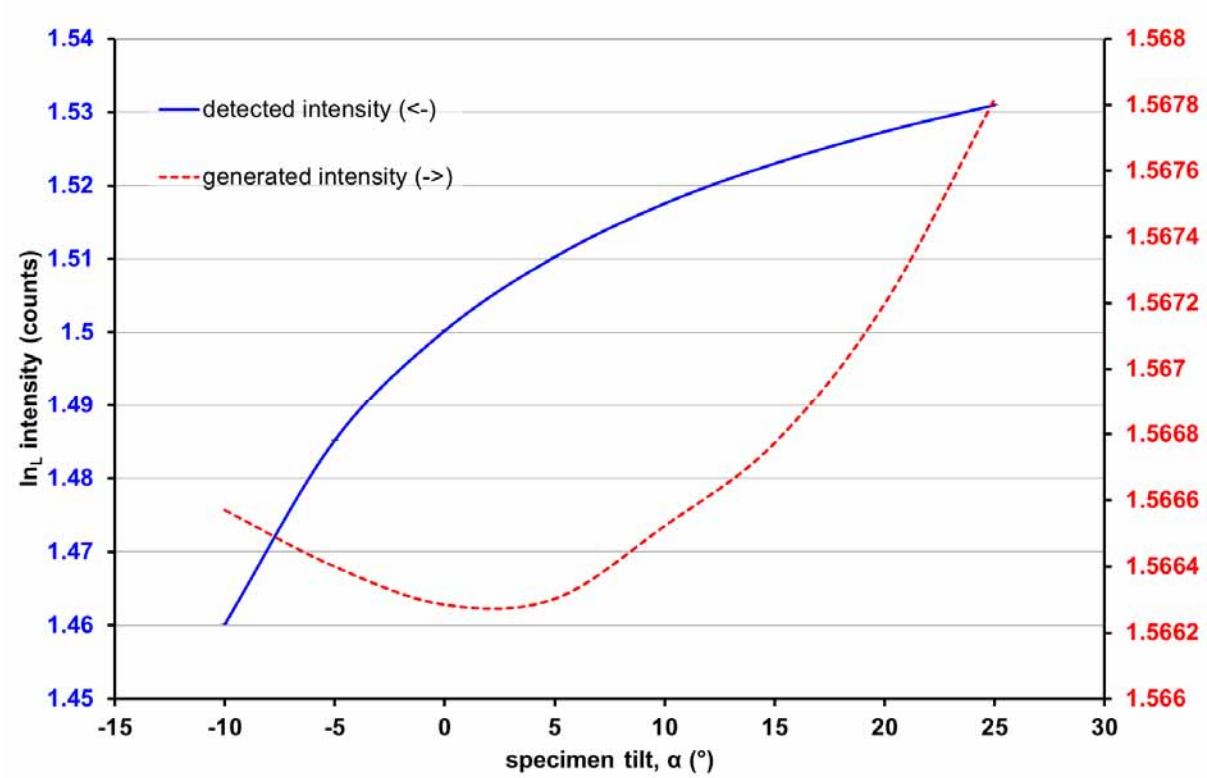

Figure 3: NISTMonte simulation results for In_L line intensity from a 1nm InAs layer embedded within a 120nm thick GaAs matrix at a depth of 50nm. Beam energy = 197keV, take-off angle of 25°. 'Generated intensity' is plotted against the secondary vertical axis to the right and refers to all X-rays produced in a tilted sample, multiplied by cos α, while 'detected intensity' includes the absorption effect due to GaAs coverage and finite take-off angle.

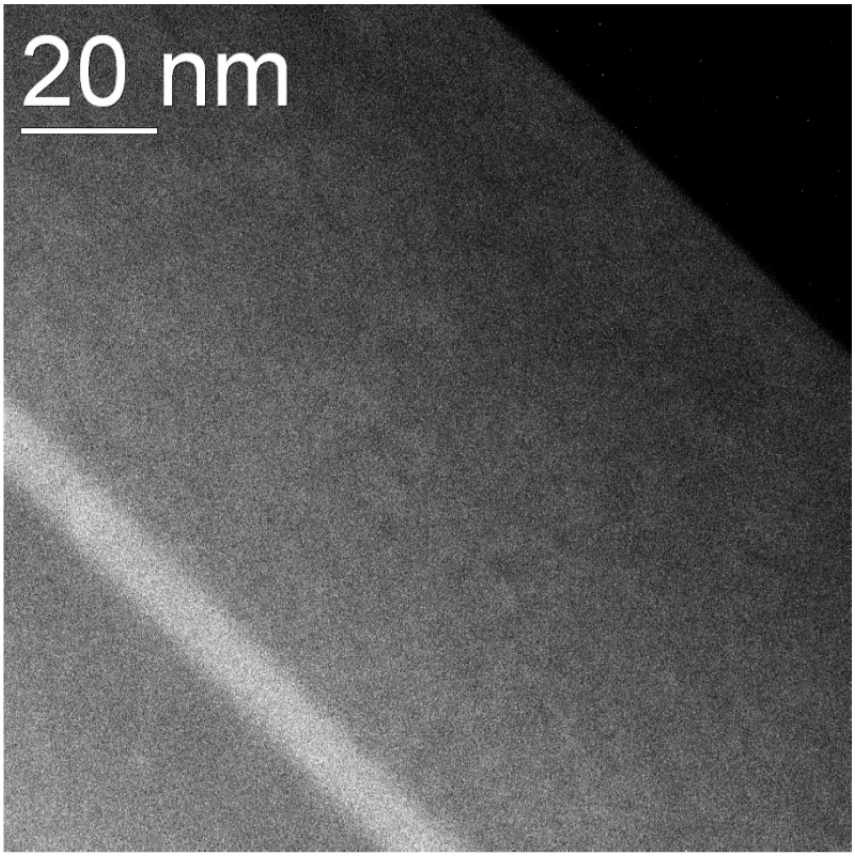

Figure 4: Cross-sectional annular dark-field (ADF) STEM image of 8nm thick $In_{0.24}Ga_{0.76}As$ layer embedded under 95nm of GaAs.

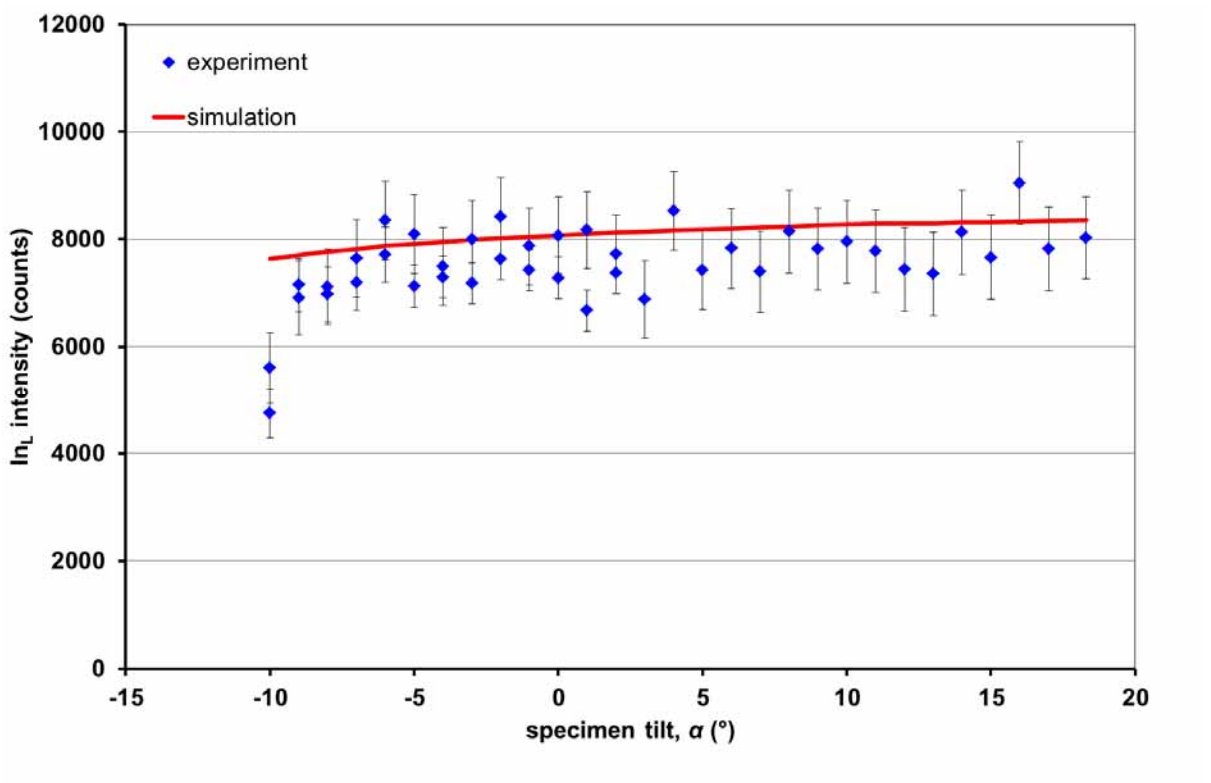

Figure 5: In_L line intensity from 8nm thick $In_{0.24}Ga_{0.76}As$ layer embedded under 95nm of GaAs. Simulation normalised with respect to experimental 0° tilt data point. $\theta = \alpha + 25°$. Simulation run in NISTMonte at beam energy 197keV with 10^6 electron histories, for an 8nm $In_{0.24}Ga_{0.76}As$ layer with a 94nm thick GaAs (density = 5.316 g cm^{-3}) overlayer.

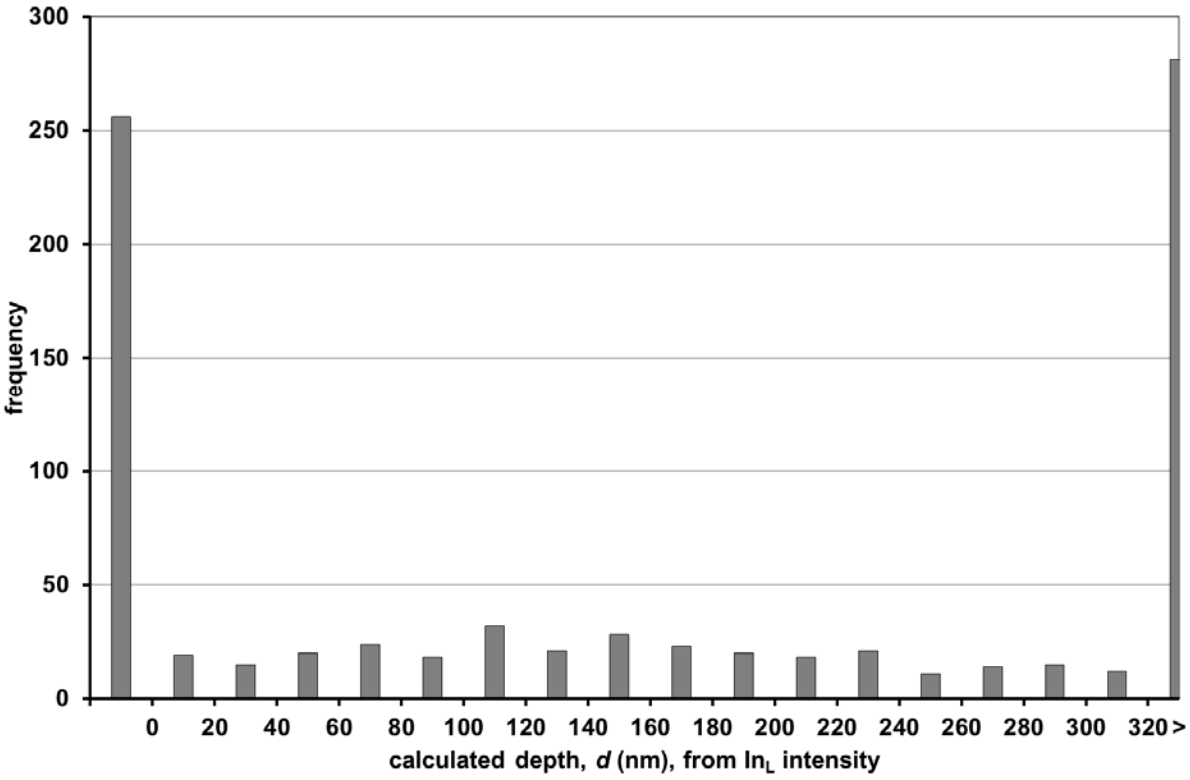

Figure 6: Result of applying equation (10b) to the data of Figure 5. λ = 2525nm. Nominal d is d_{true}=99nm. Average of all values between 0nm and 500nm is d_{exp}=200±132nm, where 46% of all data points fall into that range.

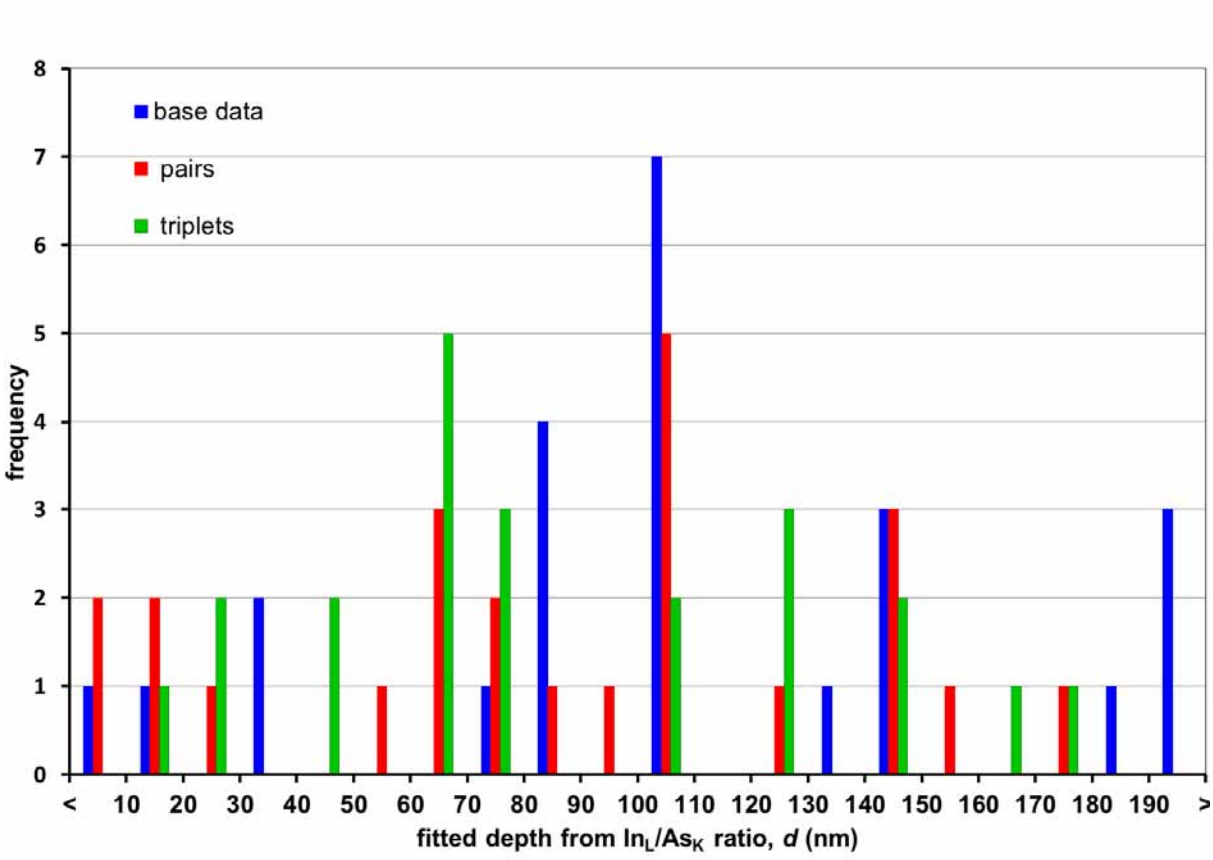

Figure 7: Histogram of results from fitting In_L/As_K simulations of varying overlayer thicknesses to experimental data. Known correct value is d = 99nm. Average overall: 95.3±50.6nm, mean error of the mean: 6.0nm. Average for 'base data': 108.5±54.4nm, mean error of the mean: 11.1nm. Average for 'pairs': 87.6±49.6nm, mean error of the mean: 10.1nm. Average for 'triplets': 89.1±46.5nm, mean error of the mean: 9.9nm.

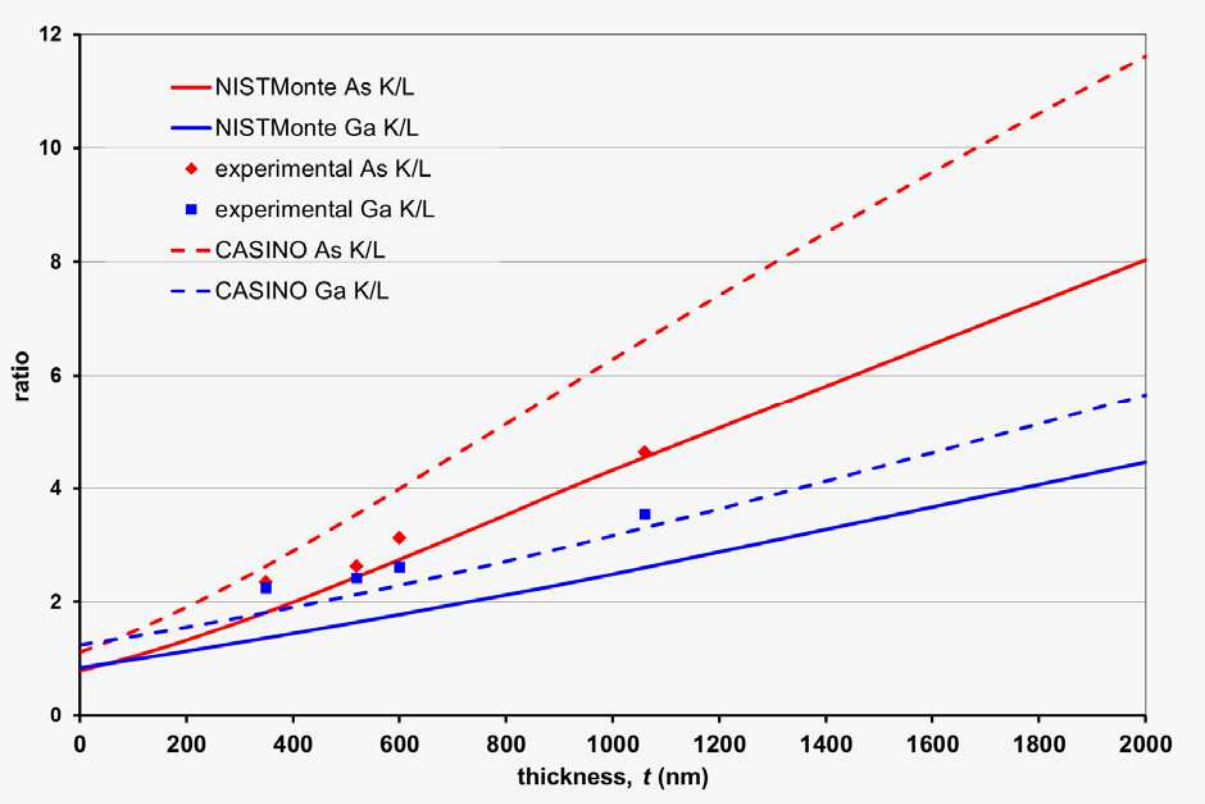

Figure 8: Comparison of NISTMonte and CASINO simulations to experimental results of K/L line intensity ratios for GaAs. Beam energy = 197keV, take-off angle of 25°.

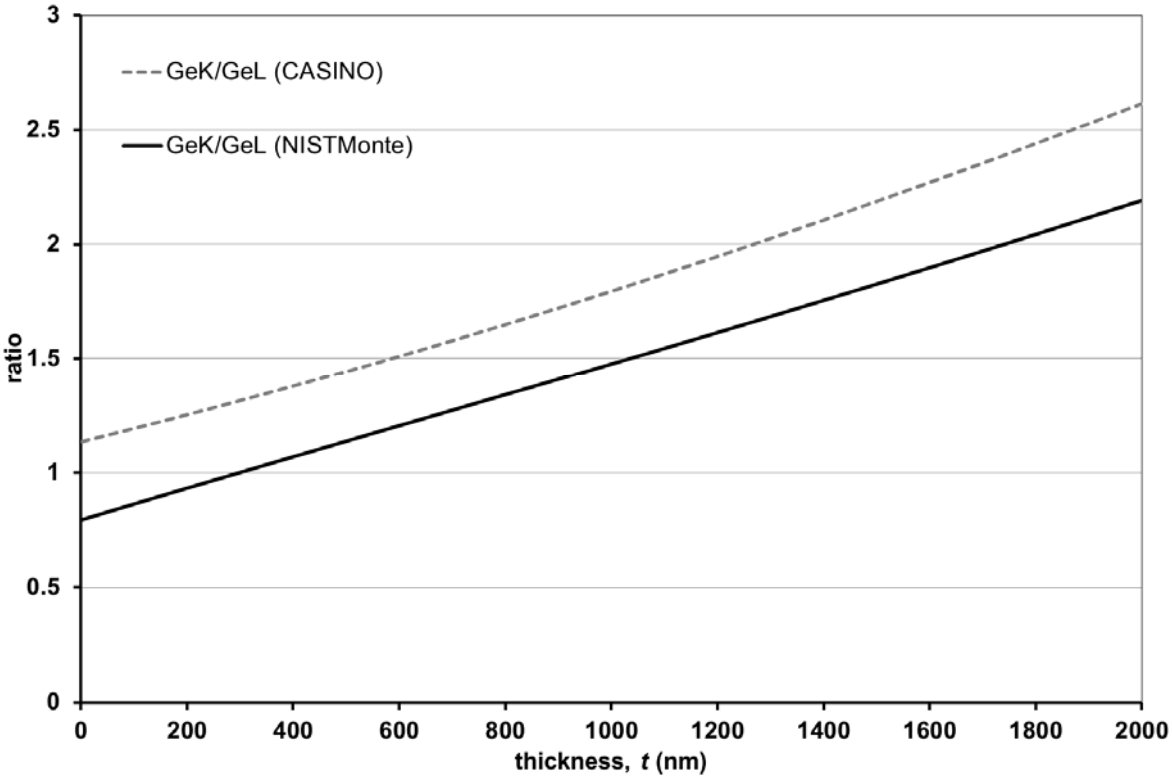

Figure 9: NISTMonte and CASINO results of K/L line ratios for $Si_{0.54}Ge_{0.46}$. Beam energy = 197keV, take-off angle of 25°, density = 3.71gcm^{-3}.

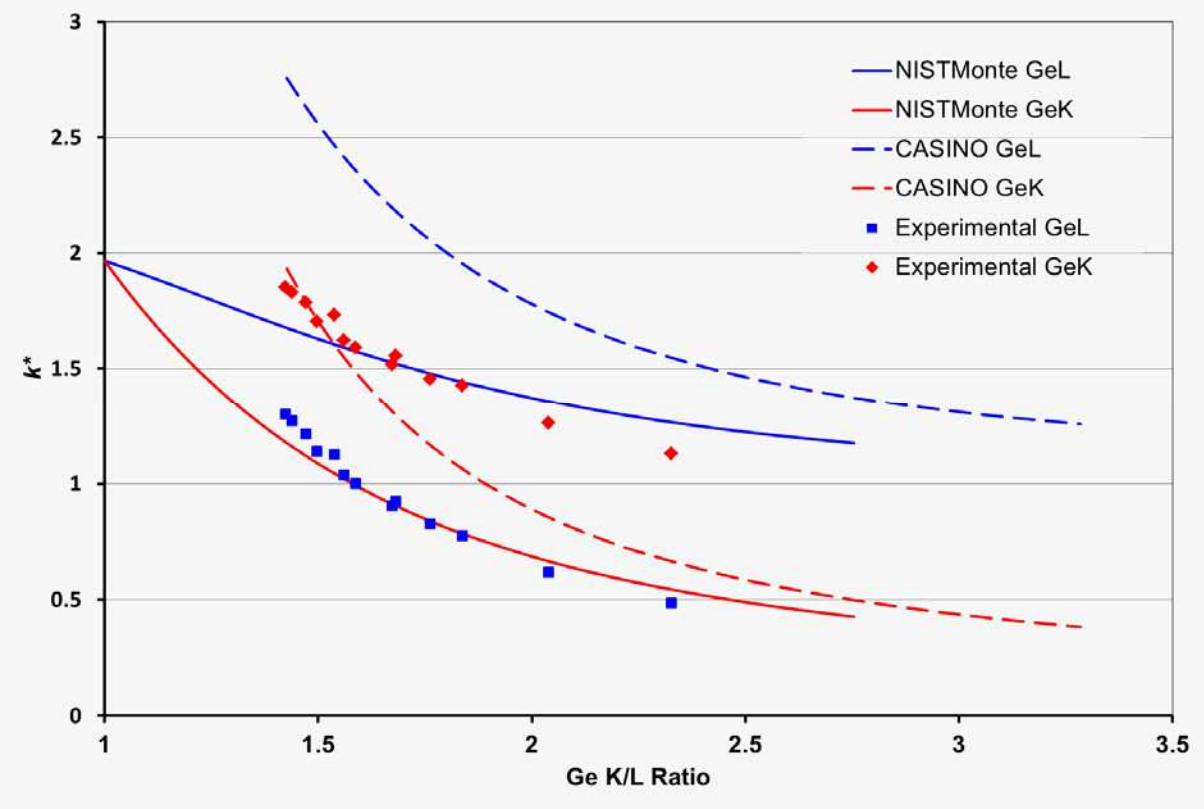

Figure 10: Comparison of simulated and experimental k^* (from equation 6) vs. specimen thickness for $Si_{0.54}Ge_{0.46}$. Beam energy = 197keV, take-off angle of 25°.

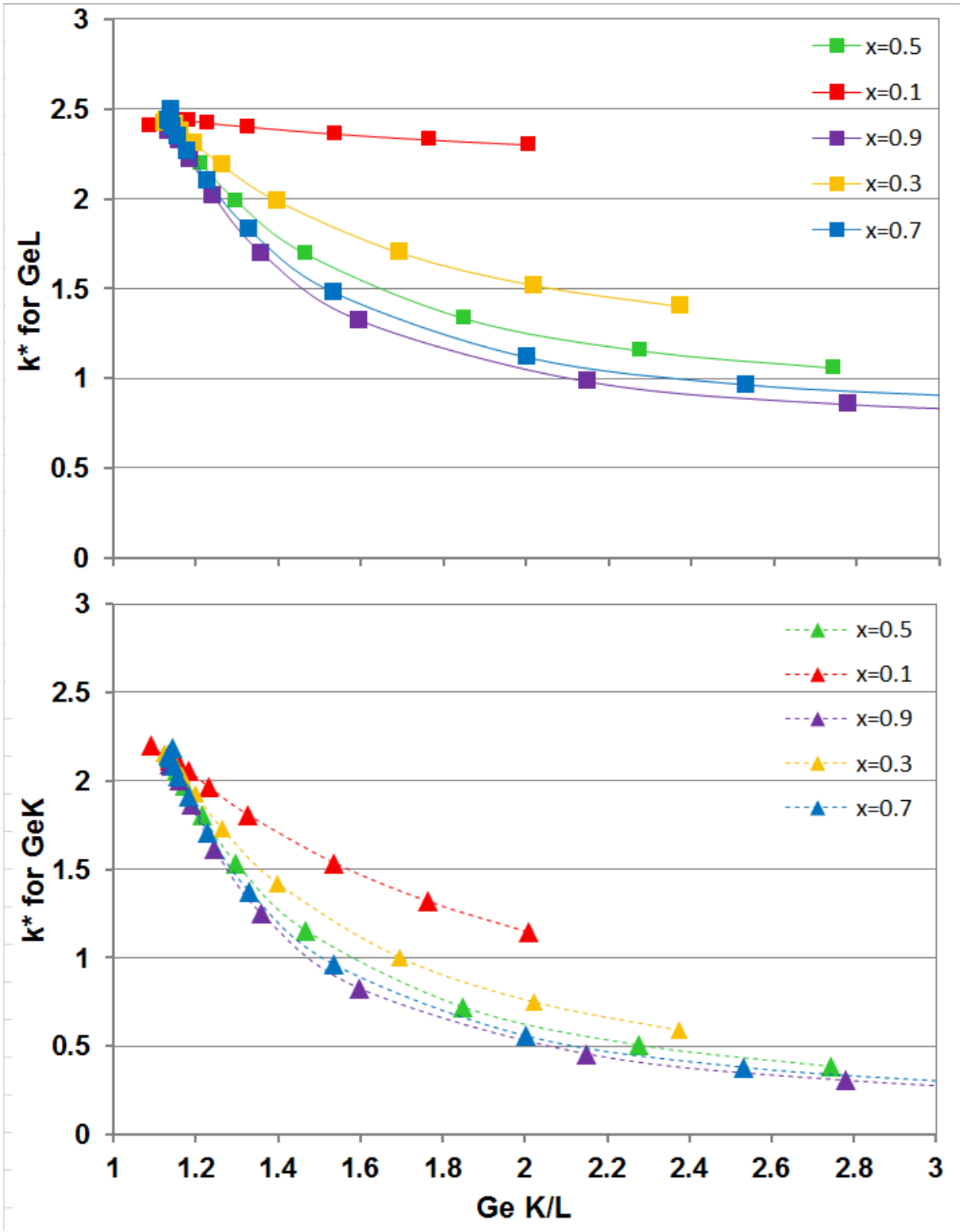

Figure 11: *k** factors simulated for $Si_{1-x}Ge_x$ alloys of different Ge content *x*. CASINO, beam energy = 200keV, take-off angle of 25°, ideal detector (*e*=1).

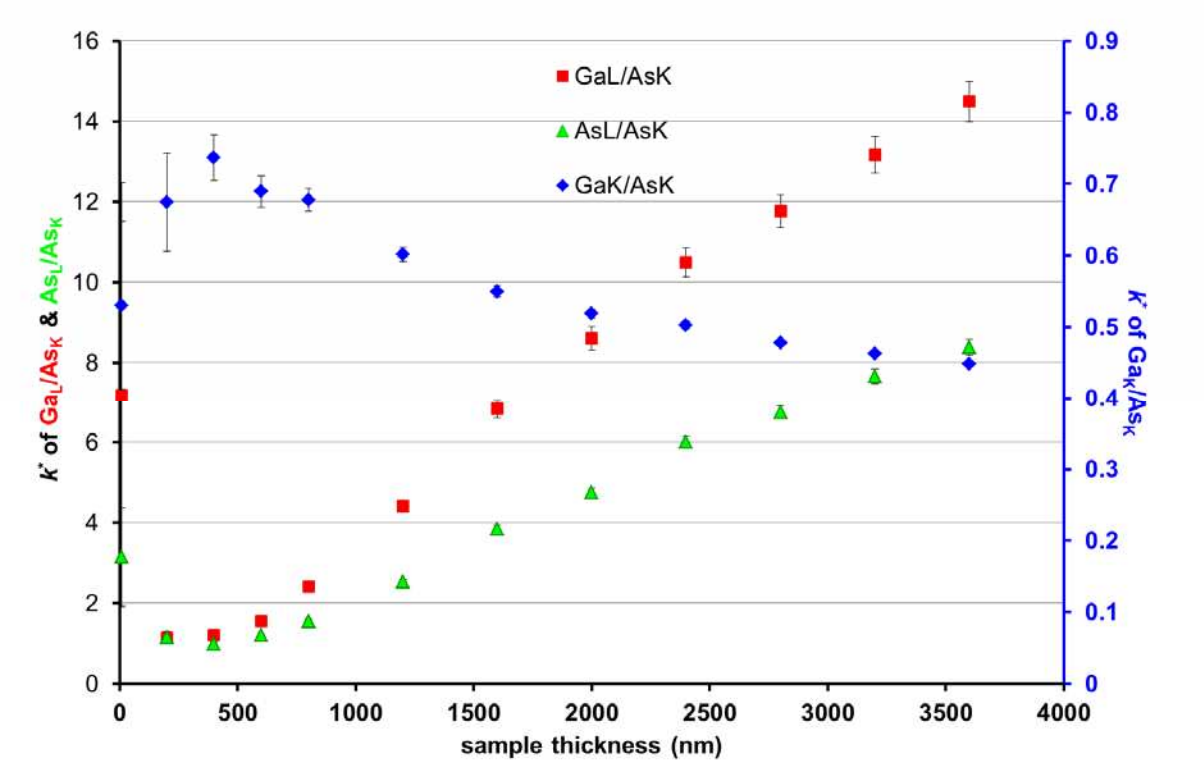

Figure 12: k^* for cleaved wedge specimen vs specimen thickness for GaAs. Ga_K/As_K is plotted against the second vertical axis on the right. The error bars of the As_L/As_K 10nm point were truncated for clarity as they extend from below zero to 54. Thickness was measured by how far the beam was moved away from the wedge's edge (thickness = twice distance from edge).

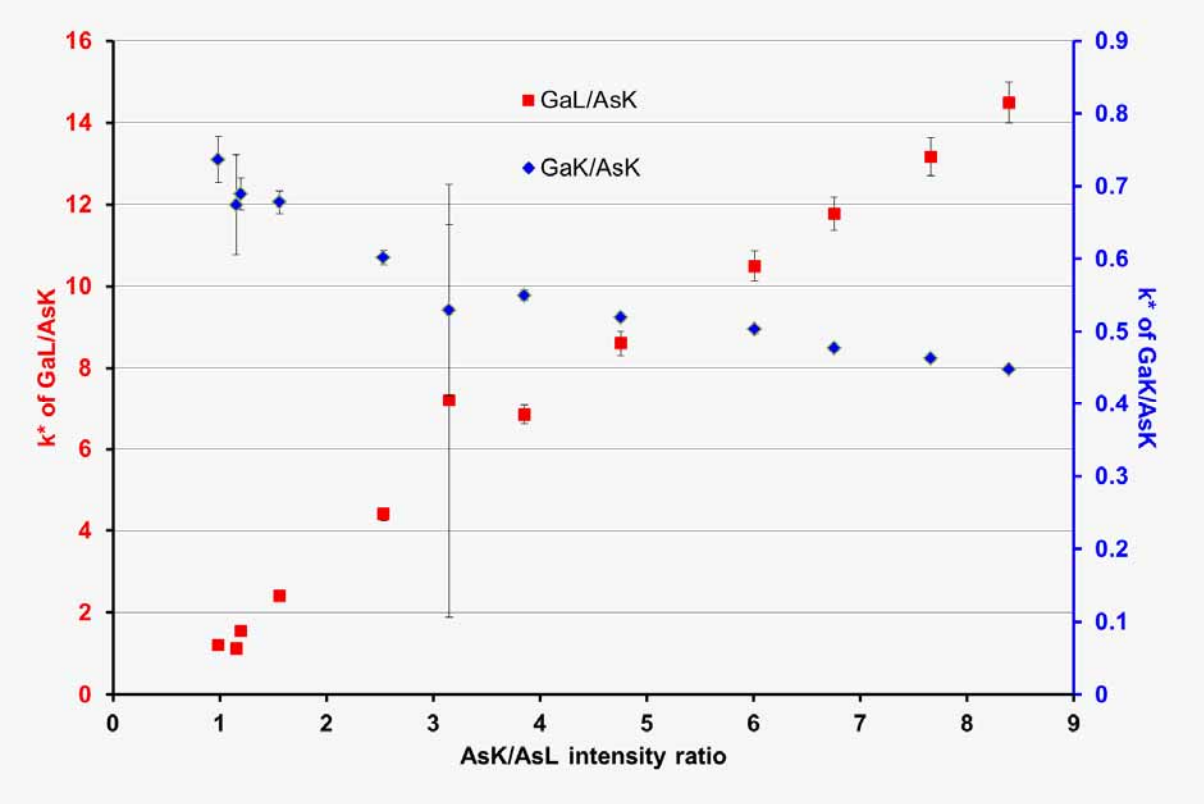

Figure 13: Experimental *k** vs. As K/L ratio for GaAs.

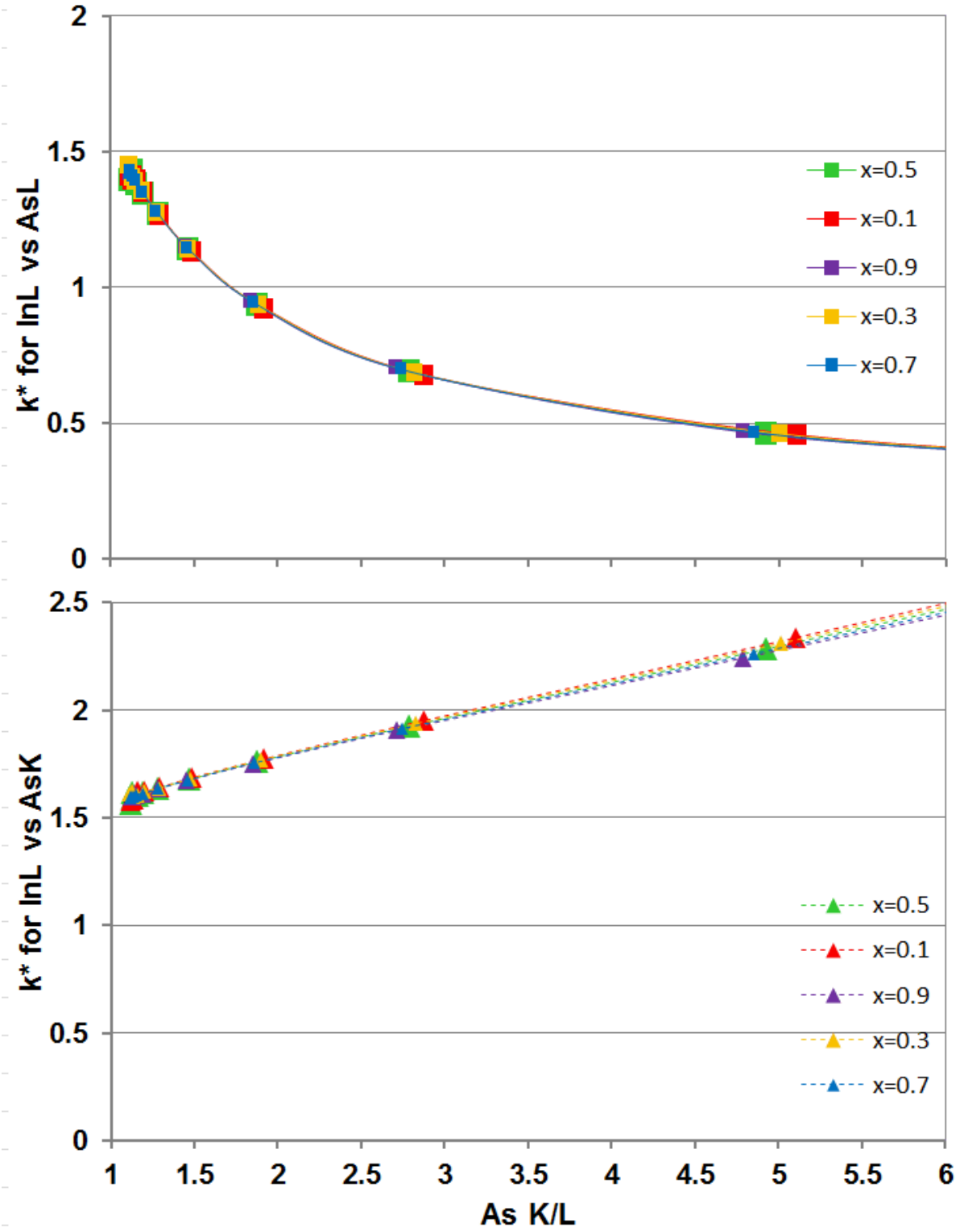

Figure 14: *k** factors simulated for $In_xGa_{1-x}As$ alloys of different In content *x*. CASINO, beam energy = 200keV, take-off angle of 25°, ideal detector (*e*=1).

Tables

X-ray line	starting energy [keV]	detector efficiency ε
Ga_L	1.10	0.65
Ge_L	1.19	0.67
As_L	1.28	0.68
Si_K	1.74	0.70
In_L	3.29	0.73
Ga_K	9.24	0.77
Ge_K	9.88	0.78
As_K	10.53	0.79
In_K	24.14	0.89

Table 1: Detector efficiencies of X-ray lines calculated by DTSA-II program (Ritchie, 2009).

		α_2 (°)						
		-5	0	5	10	15	20	25
α_1 (°)	-10	50.12	50.08	50.32	50.32	50.68	50.88	51.44
	-5		50.02	50.53	50.48	51.07	51.36	52.2
	0			51.3	50.9	51.79	52.14	53.35
	5				50.34	52.2	52.66	54.43
	10					54.75	54.48	56.82
	15						54.11	58.37
	20							63.91

Table 2: Calculated depth values d (nm) from Figure 3 and Equation (10b). Simulation run in NISTMonte (beam energy of 197keV, take-off angle of 25°, $\theta = \alpha + 25°$). The numerically correct answer would be 50.5nm for the mean depth in the foil.

intensity line ratio	slope (x10^{-3})	intercept	R^2
As_K/As_L (Experimental)	3.34±0.30	1.07±0.20	0.984
As_K/As_L (CASINO)	5.30±0.03	0.97±0.02	0.998
As_K/As_L (NISTMonte)	3.61±0.03	0.71±0.02	0.999
Ga_K/Ga_L (Experimental)	1.90±0.15	1.50±0.10	0.987
Ga_K/Ga_L (CASINO)	2.12±0.03	1.16±0.02	0.994
Ga_K/Ga_L (NISTMonte)	1.76±0.02	0.81±0.01	0.998

Table 3: Linear least-squares regression of data in Figure 8.

intensity line ratio	slope (x10^{-3})	intercept	R^2
Ge_K/Ge_L (CASINO)	0.897±0.010	1.400±0.007	0.9962
Ge_K/Ge_L (NISTMonte)	0.869±0.001	0.996±0.001	0.9998

Table 4: Linear least-squares regression of data in Figure 9.

X-ray line	ISIS *k*-factor with respect to As_K	from fig. 12, all data points included		from fig. 12, the data point at *t*=10nm excluded	
		k^* (*t*->0)	R^2 of fit	k^* (*t*->0)	R^2 of fit
Ga_K	0.877	0.68±0.04	0.679	0.77±0.02	0.949
Ga_L	0.985	1.17±0.45	0.924	0.14±0.23	0.989
As_L	1.012	2.95±1.56	0.850	-0.83±0.51	0.992

Table 5: Comparison of corrected k^*-factors with respect to As_K in GaAs.

	ISIS *k*-factors with respect to As_K	from fig. 13, against As_K/As_L		from fig. 12, against Ga_K/Ga_L	
X-ray line		k^* (t->0)	R^2 of fit	k^* (t->0)	R^2 of fit
Ga_K	0.877	0.73(2)±0.00(6)	0.975	0.70(4)±0.00(4)	0.956
Ga_L	0.985	0.81±0.05	0.992	1.05±0.05	0.999
As_L	1.012	1	1	2.10±0.16	0.992

Table 6: Comparison of corrected k^*-factors with respect to As_K. Intensity ratio at t = 0 taken from Table 5.